A Miniaturised UV Imaging Spectrometer for Remote Sensing of Atmosphere: Volcanic Sulphur Dioxide, Ozone, and Aerosols

Juan A. Fernandez-Saldivar

Abstract A new compact and low-cost high spectral resolution imager for selected ultraviolet bands is proposed to operate in a micro-satellite constellation with the objective of monitoring important atmospheric constituents: sulphur dioxide (SO_2), ozone (O_3) and aerosols. The spectral resolution and imaging performance of the sampled spectra are studied, given the distortions observed from different angular fields to estimate the slit function. Radiative transfer simulations using MODTRAN with the derived resolution will show the differential radiances under various scenarios with SO_2 "clean" and "contaminated" atmospheres. The instrument design exploits the excellent response of new silicon carbide photodiodes in this region; its blindness to visible radiation provides for a relatively simple and compact optical design ($9 \times 13 \times 6$ cm). The use high-efficiency transmission gratings and 20-bit electronics (consuming less than 5 W) offer high sensitivity. Other wavelengths outside this region (331 nm and 360 nm) are sampled at a ground distance of 7×32 km, so that the presence of aerosols may be detected, and the background UV albedo can also be determined for retrieval algorithm purposes.

1 Introduction

Currently observations in the UV region are restricted to large platforms and instruments such as NASA's Total Ozone Mapping Spectrometer (TOMS) and Ozone Monitoring Instrument (OMI) and ESA's Global Ozone Monitoring Experiment (GOME) and Scanning Imaging Absorption Spectrometer for Atmospheric Cartography (SCIAMACHY). With the exception of TOMS, which was not designed to monitor SO_2 and still holds an unrivalled record in detecting volcanic activity [1], all the others face various trade-offs when observing the UV spectrum between 300 and 315 nm wavelength. Because of the wide dynamic range of backscatter

J.A. Fernandez-Saldivar
Surrey Space Centre, University of Surrey, Guildford, Surrey, GU2 7XH, UK
e-mail: j.fernandez@surrey.ac.uk

R. Sandau et al. (eds.), *Small Satellites for Earth Observation*,

radiation observed, it is common to optically split this region in to two ranges and use detectors with differing sensitivity (Fig. 1 Left), thus degrading the signal to noise ratio. This split occurs precisely in a region where the SO_2 absorption features provide easier discrimination with respect to O_3 and this can lead to problems in the retrieval algorithms.

2 Spectral and Radiometric Analysis

The spectral range and resolution required to discriminate SO_2 from O_3 is defined by the absorption spectra of these trace gases. In the region between ∼300 and 320 nm SO_2 absorption is greater than O_3 (Fig. 1 Right). However it is below ∼313 nm, where the ozone absorption is smooth, that SO_2 features are more easily identifiable for discrimination. SO_2 shows a wave-like spectrum with peaks and troughs evenly spaced every ∼1 nm (spectral sampling) and with an estimated Full Width Half Maximum (FWHM) of ∼0.4 nm (spectral resolution). We can therefore use these peaks and troughs to obtain information on the ratio of SO_2 to O_3 (Fig. 1 Right inset). Above ∼313 nm the features would require higher spectral sampling and resolution.

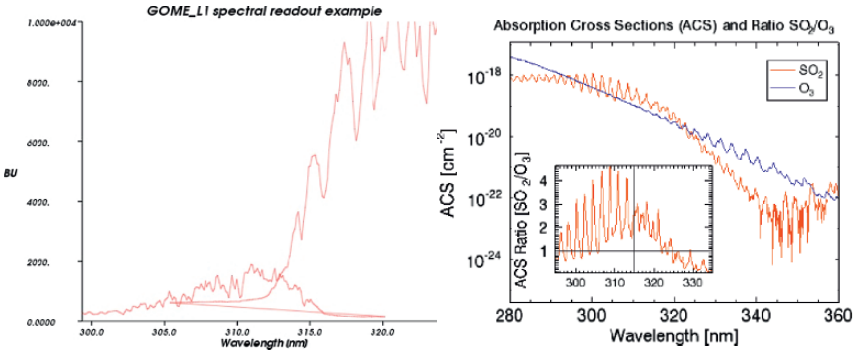

Fig. 1 (*left*) UV channel overlap for GOME [2]. (*right*) absorption cross sections for SO_2 at 243K [3] and O_3 at 241K [4]. (*right* Inset) ACS ratio of these constituents for discrimination

In order to estimate the radiometric resolutions required, a radiative transfer model was computed using MODTRAN [5] under these conditions: Tropical Atmospheric standard profiles, no aerosols, no clouds and solar angle of 25 degrees. Atmospheres with three ozone concentrations were analysed, each "contaminated" with an SO_2 layer of varying concentration at 4 km scale height (Fig. 2).

By taking the ratios of radiances obtained by from the atmosphere with varying amounts of SO_2 and O_3 with respect to those obtained from a standard no-clouds tropical atmosphere (no SO_2, and 277 DU of Ozone), we can observe the different spectral signatures of these trace gases. As expected from its Absorption Cross Section we observe in Fig. 3 the jagged behaviour of SO_2 (Left) compared to the smooth

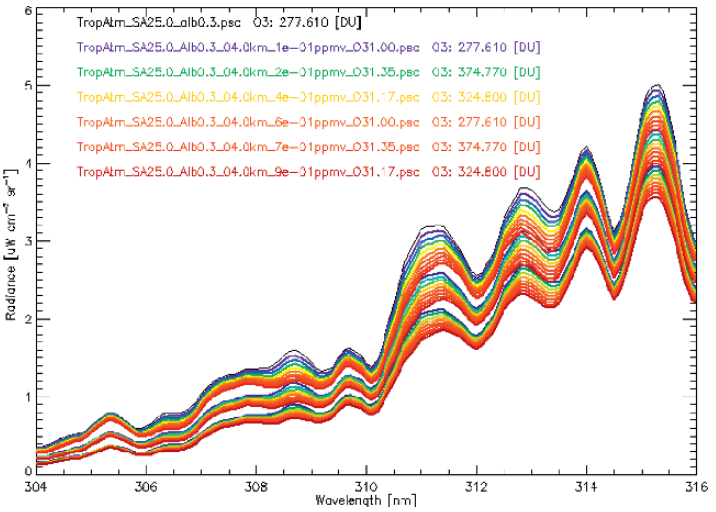

Fig. 2 Radiative transfer simulations for SO_2 contaminated atmospheres under 3 different O_3 conditions

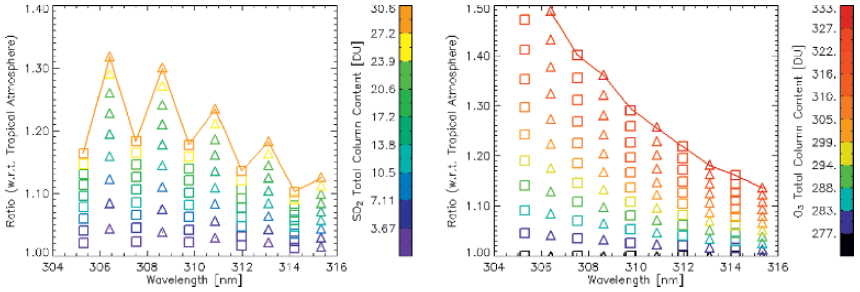

Fig. 3 Radiance ratio w.r.t. tropical atmosphere (*left*) atmosphere affected by SO_2 (*right*) affected by O_3

curves due to O_3 (Right). These features will allow the discrimination of these two gases using retrieval techniques such as the Band Residual Difference algorithm [6].

3 Instrument Design

The instrument was designed to obtain a ground sample distance at nadir of 4×30 km; this is considered useful according to the Disaster Management Support Group (DMSG) of the Committee on Earth Observation Satellites (CEOS) suggesting 10 to 20 km [7]. The calculated spatial resolution is half the area covered by a normal OMI pixel (12×24 km) and 20 times smaller than TOMS (50×50 km); it is expected to minimise cloud cover scenes and increase the sensitivity in detecting

SO_2 contaminated pixels. A medium swath (~300 km) for a single imager would require the use of two imagers in order to observe large drifting clouds and reduce the revisit time; it would also match the Disaster Monitoring Constellation of micro-satellites imager pair swath [8]. The challenging requirements of the application such as: wide dynamic range and low-noise demand an extremely low circuit noise matched to a highly sensitive detector to ultimately define the system sensitivity. For this purpose a low power (<5 W) electronic solution comprising a switched integrator and 20-bit Analog-to-Digital converter in a miniature device is proposed.

3.1 Optics

The optical layout was chosen to have minimum number of parts whilst maximising the optical throughput (etendue). It uses the largest commercially available holographic transmission grating, matching it with a custom-made area array of Silicon Carbide (SiC) photodiodes at the focal plane. The use of fused-silica lenses will provide good transmission and performance in the UV, and some optical surfaces have an aspherical design to minimise distortions. The optical design was optimised around the central wavelength at 310 nm because of the critical requirements in this region. The performance of auxiliary channels is not as critical because the spectral resolution needed in those channels is not as demanding as in the continuous region. The layout proposed is shown in Fig. 4 below. On top we observe the three main optical rays of the three wavelength regions, 360 nm, 331 nm and 305–315 nm (left to right.)

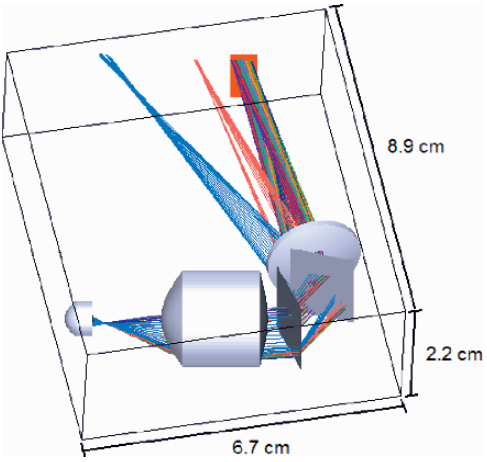

Fig. 4 Optical layout

3.2 Grating and Detector

Two key elements were the main drivers of the design: the transmission grating size (15 × 20 mm) and the pixel size of the photodiode array (0.4 × 0.6 mm). Transmission

gratings with high efficiency will provide the spectral dispersion required. An area array of Silicon Carbide (SiC) photodiodes is proposed because it is naturally blind to visible radiation. The combination of these two yields the spectral resolution and sampling required for the application. This is observed in Fig. 5, which shows the spectral imaging characteristics at the focal plane with its relative illumination and spectral resolution.

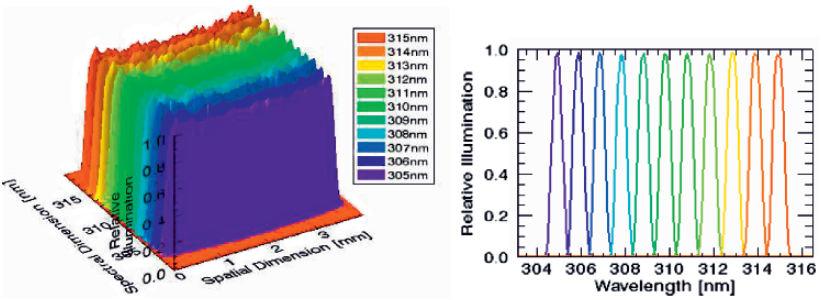

Fig. 5 (*left*) Spectral imaging at focal plane. (*right*) spectral resolution at 11 wavelengths

One area array of SiC photodiodes consisting of 10 × 10 pixels is proposed for the 10 contiguous channels (305–315 nm). Two linear arrays of 10 × 1 pixels will be used in the auxiliary channels 331-nm and 360-nm for determination of ozone products, aerosols and UV albedo.

The spectral imaging of all channels is shown in Fig. 6 below for the chief rays passing through the centre of the entrance pupil. A grid distortion is observed on all 3-wavelength ranges and a spectral "smile" causes the image to curve up as it approaches the edges of the detector arrays. However, this distortion is minimal for the chief rays.

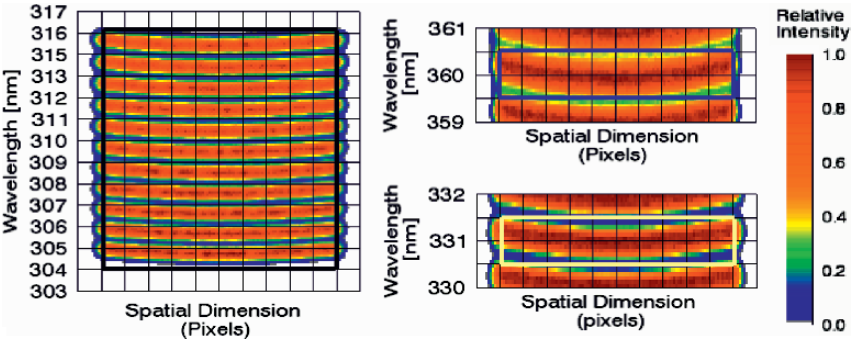

Fig. 6 Spectral imaging at focal plane. (*left*) detector array 305–315 nm (*right*) auxiliary channels 331 nm and 360 nm

The illumination on the focal plane is also analysed by considering the marginal rays passing through the entrance pupil from 2° to 14°. The real IFOV of the

spectrometer is 12.7° however a wider view is tested to test for influence on the spectral characteristics. This is shown in Fig. 7 for the chief rays (left) and for all rays including marginal rays (right).

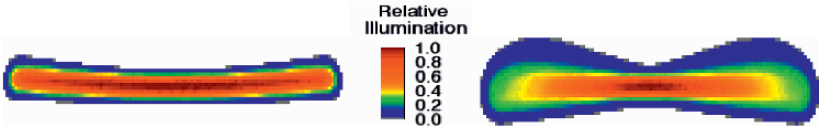

Fig. 7 Spectral imaging illumination @ 310 nm (*left*) ±2° fields. (*right*) ±12.7° fields

Slicing the above relative illumination images vertically at 10 different locations corresponding to the detector array columns, we obtain a Gaussian-like curve (Fig. 8).

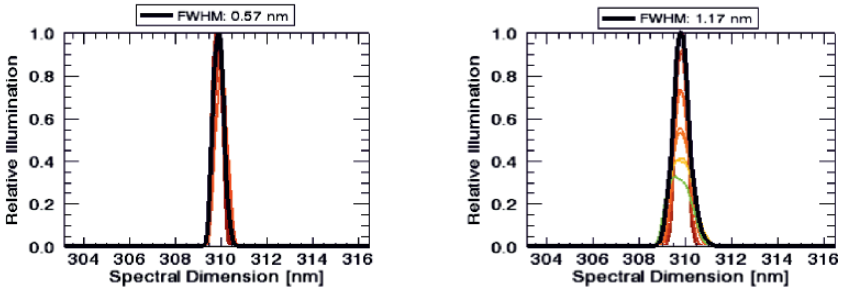

Fig. 8 Full width at half maximum (FWHM) @ 310 nm (*left*) ±2° fields. (*right*) ±12.7° fields

Once the real FWHM defined by the slit function has been obtained for all fields in the focal plane, the radiance ratios are computed by convoluting the spectral radiance with the appropriate slit function. The inclusion of marginal rays reaching the edge of the entrance pupil Fig. 9 (right) shows the reduction in the apparent "modulation" of the spectrum, with respect to that obtained with the chief rays alone (left). The Left graph is representative of the very best performance we could expect from the instrument on the optical axis, whereas the Right graph is representative of the overall instrument performance.

The marginal ray analysis allows determination of spectral and spatial distortions in terms of variations in the expected FWHM and the relative position of the wavelengths as the marginal rays reach the edge of the entrance pupil (Table 1).

The changes in relative intensity are a result of vignetting; however the absolute expected levels of radiance should still meet the optical signal requirements of the algorithm (0.01 μW cm^{-2} sr^{-1} threshold). The widening of the FWHM and the resulting offset will combine to degrade the sensitivity at the edges of the FOV. However, it is proposed to use two instruments in a similar way to the way the DMC imagers are operated, giving an optical axis which is tilted ∼12° off-nadir. This counteracts the degradation to some extent over the central portion of the image. At the edge of the swath of the imaging pair, the lack of sensitivity will greatly reduce the performance.

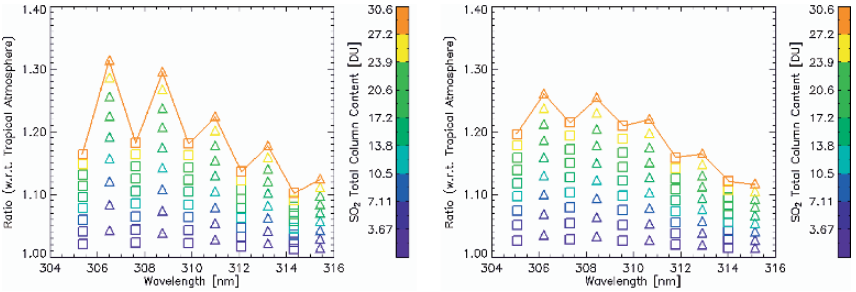

Fig. 9 Radiance ratio w.r.t. tropical atmosphere (*left*) $\pm 2^\circ$ fields with FWHM = 0.57 nm. (*right*) $\pm 12.7^\circ$ fields with FWHM = 1.17 nm

Table 1 Spectral and spatial changes in FWHM and position

Field [degrees]	Relative Intensity	Spectral Position [nm]	Spectral FWHM [nm]	Spatial Position [mm]	Spatial FWHM [mm]	Abs. wav offset [nm]	Position offset [mm]
0	1	309.8746	0.5403	2.9388	0.2406	0.0000	0.0000
2	0.923396	309.8609	0.5712	2.9449	0.2544	0.0138	0.0061
4	0.761339	309.8235	0.6668	2.9616	0.2969	0.0511	0.0228
6	0.590644	309.7750	0.8132	2.9832	0.3621	0.0996	0.0444
8	0.469599	309.7188	0.9734	3.0082	0.4335	0.1559	0.0694
10	0.380238	309.6503	1.1038	3.0387	0.4915	0.2243	0.0999
12	0.315583	309.5621	1.1727	3.0780	0.5222	0.3125	0.1392

This is a condition all spectral imagers face to some extent and it is a design trade-off we cannot easily avoid without adding optical complexity to the instrument.

If we consider the variations in FWHM along the spectral dimension we observe these are a minimum in the detector array covering 305–315 nm. On the auxiliary channels (331 nm and 360 nm) the performance is degraded due to the widening of the slit function. This occurs because the optical design is aimed at producing the best optical performance at the shorter wavelengths which have lower radiances. However, despite this compromise, the overall instrument performance of the instrument meets the requirements of the application in mind. Table 2 below summarizes the results obtained for representative wavelengths.

Table 2 Spectral and spatial changes in FWHM and position

Wavelength Band [nm]	Relative Intensity	Spectral Position	Spectral FWHM [nm]	Spatial Position [mm]	Spatial FWHM [mm]	Wavelength offset [nm]
305	0.962532	304.9648	0.5149	5.1252	0.2293	0.0353
310	0.957696	309.8746	0.5403	2.9388	0.2406	0.1254
315	0.969093	315.0067	0.5639	0.6534	0.2511	−0.0067
331	1	330.9560	0.5397	2.9066	0.2909	0.0440
360	0.922996	359.9814	0.6851	2.8727	0.4817	0.0186

The expected instrument specifications are shown in Table 3 below.

Table 3 Instrument Specifications

Field of View	$25.8^\circ \times 0.57^\circ$
Pixel Size	0.4×0.6 nm
Pixel sample distance	7×31.5km[§]
Revisit Time	Daily *
Spectral Resolution	0.5–1.1 nm/0°–12°
Slit	6×0.100 mm
Grating	2847 lines mm^{-1}
Etendue	7.48×10^{-4} sr^{-1} cm^{-2}
S/N @ 0.1 uW $sr^{-1}cm^{-2}$	~244 (on axis)
Entrance Pupil Diameter	4 mm
Back Focal Length	60.17 mm
Working F/#	6.33

[§]single imager
**dual UV-Imager on DMC-type constellation*

4 Conclusions

The instrument is designed in order to meet the rapid response and dynamic requirements of demanding applications such as volcanic activity monitoring. The demanding requirements to consider when designing such a system were shown indicating the potential of such instruments to successfully detect and discriminate two important trace gases: SO_2 and O_3. The auxiliary channels may also be used to determine the concentration of aerosols.

The optical design and its spectral imaging properties across its field-of-view were discussed together with the requirements of various atmospheric scenarios and imaging characteristics. The instrument imaging performance fulfils the application needs according to radiative transfer simulations of realistic atmospheric scenarios. The detection limits, based on the expected detector performance, are aimed ideally to observe minor concentrations of SO_2 produced by passively outgassing volcanoes $\leq$5 DU and certainly should be capable of monitoring volcanic events releasing $>$10 DU. However, the real detectivity will be defined once the noise performace of the electronics have been tested and verified.

The relatively low-cost and small size of the instrument proposed makes it a suitable instrument for a micro-satellite-based atmospheric remote sensing mission.

References

1. Carn, S.A., Krueger, A.J., Bluth, G.J.S., Schaefer, S.J., Krotkov, N.A., Watson, I.M., Datta, S., *Volcanic eruption detection by the Total Ozone Mapping Spectrometer (TOMS) instruments: a 22-year record of sulfur dioxide and ash emissions*, in *Volcanic Degassing*, C. Oppenheimer, Pyle, D. M., Barclay, J., (Eds.) 2003, Geological Society: London. pp. 177–202.

2. ESA, *Basic ENVISAT Atmospheric Toolbox (BEAT)*. 2006, European Space Agency.
3. Bogumil, K., Orphal, J., Burrows, J.P., *SO2 Absorption Cross Sections at 243K – version1.0*. 2000, Institute of Environmental Physics – University of Bremen: Bremen, Germany.
4. Burrows, J.P., Richter, A., Dehn, A., Deters, B., Himmelmann, S., Voigt, S., Orphal, J., *Atmospheric remote-sensing reference data from GOME. Part 2. Temperature dependent ACS of O2 in the 231–794 nm range.* Journal of quantitative spectroscopy and radiative transfer, 1999. **61**: pp. 509–517.
5. Berk, A., Anderson, G.P., Acharaya, P.K., Hoke, M.L., Chetwynd, J.H., Bernstein, L.S., Shettle, E.P., Matthew, M.W., Adler-Golden, S.M., *MODTRAN 4 Version 3 Revision 1 User's Manual*. 2003, Air Force Research Laboratory.
6. Krotkov, N.A., Carn, S., Krueger, A. J., Bhartia, P. K., Yang, K., *Band residual difference algorithm for retrieval of OS2 from the Aura Ozone Monitoring Instrument (OMI).* IEEE transactions on geoscience and remote sensing, 2006. **44**(5): pp. 1259–1266.
7. CEOS, *Team Report: VOLCANO (Final Report)*, C.D.M.S. Group, Editor. 2001.
8. Underwood, C.I., Mackin, S., Stephens, P., Hodgson, D., Da Silva Curiel, A., Sweeting, M., *Evaluation of the utility of the Disaster Monitoring Constellation in support of Earth Observation Applications*. in *Small Satellites for Earth Observation*. 2005, Berlin, Germany: Walter de Gruyter.